Assessment of Castigliano's Theorem on the Analysis of Closing Loop for Canine Retraction by Experiment and Finite Element Method. Part I

Varintra Ungbhakorn
Department of Orthodontics, Faculty of Dentistry
Chulalongkorn University, Bangkok 10330, Thailand
Tel: (662) 218-8754
E-mail: nchudhabuddhi@hotmail.com

Variddhi Ungbhakorn
Mahanakorn University of Technology, Nong Chok, Bangkok 10530, Thailand
Tel: (662) 218-6629
E-mail: fmevub@eng.chula.ac.th
Corresponding author

Paiboon Techalertpaisarn
Department of Orthodontics, Faculty of Dentistry
Chulalongkorn University, Bangkok 10330, Thailand
Tel: (662) 218-8951
E-mail: gonggort2@hotmail.com

Abstract

In Part I, the Castigliano's theorem is applied to derive the equations for the ratios of M/F and loop stiffness for four types of closing loop, namely, the vertical helical loop, T-loop, Opus90 loop, and helical T-loop. The last type of loop is a new design offered in this study. The theoretical M/F is maximized to yield the optimum closing loop configurations for canine retraction where their heights and widths are limited to 10x10 millimeters. For closing loop applications, certain serious assumptions required by the Castigliano's theorem are violated, therefore, accuracy in theoretical prediction is not expected. However, trends indicating the influences of various variables leading to the optimum design of each loop type coincides with the observations of several researchers in the past. These optimum configurations will be used to study experimentally in Part II. Since the facility for determining M/F by experiments is not available, only experimental results on loop stiffness will be compared to those obtained by Castigliano's theorem and a finite element method (FEM). If the FEM yields good prediction of the loop stiffness within allowable discrepancy, then, the M/F resulting from FEM may be used for actual estimates, even though it requires future experimental verification.

Keywords: closing loop, canine retraction, Castigliano's theorem, finite element method

1. Introduction

Bodily movement or translation of a partially restraint body such as a tooth or a group of teeth occurs only if the line of force acts through its center of resistance or CRE [1]. The position of CRE for each tooth depends on its size, shape and supporting tissue, etc. [2,3]. If bodily movement could be achieved, the level of stress and strain of the supporting structure of the tooth roots can be minimized. Unfortunately, in reality, the position of the CRE is such that it is impossible to obtain a bodily movement by

using a single force, hence, a system of force consisting of forces and moments must be applied to the brackets bonded to the crowns instead. There are two methods in moving a tooth or a segment of teeth [1,4]. The first method is called sliding mechanics and the second, loop mechanics. The latter method is our interest in this paper. The method involves the application of a system of force in bending arch wire into loops of various configurations in continuous arch wires to deliver the appropriate M/F to the tooth or a group of teeth when being activated. These loops are called closing loops. To design the closing loop to deliver the desired M/F with proper loop stiffness K (loop applied force per unit deflection or the slope of the graph of force vs. deflection) is the most difficult task for a successful movement of a tooth. If the value of the loop stiffness is high, then a large magnitude of force is needed to activate one millimeter of the loop legs. For example, if the loop stiffness K is equal to 200 gm/mm (1.962 N/mm), then to activate 2 millimeters, a force equivalent to 400 gm (3.92 N), is required at the loop legs. The high force magnitude may hurt the patient because of high stress at the periodontal ligament. Also the rate of force decay will be rapid and hence more frequent activation is needed than a loop with lower stiffness. Some orthodontists choose to reduce loop stiffness by using costly arch wire with a lower value of Young's modulus [5-7] such as TMA arch wire.

As mentioned above, translation of a tooth can occur only when the line of action of force passing through CRE. But, in a real situation, we can apply force to a tooth through the bracket bonded on the crown only. If the distance between the bracket and CRE is equal to d, then an undesirable moment, M = F x d, arises. The concept of the closing loop is to generate a moment with a magnitude equal and opposite to the undesirable moment so that a pure translation can be realized. Hence, the ideal ratio of M/F of the closing loop must be equal to d, the distance between the bracket and CRE. In the past many researchers [1,2,8-12] tried to determine this distance and came to the conclusion that the distance d for the maxillary is between 7.6 to 9.6 millimeters, and the mandibular, 7.6 to 10.3 millimeters.

Several loop configurations believed to yield high ratio of M/F and used by orthodontists are: vertical helical loop, T-loop, and L-loop. None of these loops is capable of giving the required inherent ratio of M/F. Therefore gable bends anterior and posterior to the loop legs are needed to obtain a ratio of M/F of about 8 to 10 millimeters. Siatkowski [1,8] studied and designed new configurations of loops, the Opus90 and Opus70, but still the maximum inherent ratio of M/F is only about 5.5 millimeters when loops are centered between brackets. But if the Opus70 is located off-center with a distance from the anterior leg to the bracket of 1.5 millimeters, he could obtain a value of M/F close to the desired magnitude for the tested wire size. Such an arrangement is rather difficult in practice. Furthermore, once the wire size changed, the M/F becomes an unknown again.

It can be seen that if a reliable analytical or numerical method of the closing loop analysis is available, then any orthodontists can use this tool to calculate the characteristic of their closing loops theoretically without resorting to costly and time-consuming experiments. In this first part of the paper, the authors employ the existing Castigliano's theorem to derive the expressions for the loop stiffness and ratios of M/F for various loop configurations. To determine M/F experimentally is costly, and it is rather difficult to obtain accurate results due to its small size as compared to the sensor such as a strain gage. Therefore to check the validity of the theoretical results, only experimental results of the loop stiffness will be compared in Part II. Only the optimum design of each loop configuration obtained from using the Castigliano's theorem in Part I will be used to study in part II of the paper employing the finite element method. If FEM can predict the values of the loop stiffness to within an acceptable discrepancy, then we may assume that the computed ratio of M/F by FEM can be used to estimate the actual values also.

2. Material and Methods

2.1 Castigliano's theorem

In 1879, Alberto Castigliano, an Italian railroad engineer, outlined a method for determining the displacement and rotation at a point in a body. This method, which is referred to as Castigliano's second theorem, applies only to bodies that have constant temperature and

material with linearly elastic behavior. The theorem states that [13]:

The first partial derivative of the strain energy in the body with respect to a force (or moment) acting at the point is equal to the linear displacement (or angular displacement) of that point in the direction of force (or moment).

In mathematical form, it can be written as:

$$\delta_n = \frac{\partial U}{\partial P_n} \qquad (1)$$

where U is the strain energy of the elastic body and if P_n represents a force, then δ_n becomes the linear displacement, but if P_n represents a moment or couple, then δ_n becomes the angular displacement.

In order to apply Castigliano's theorem successfully the following assumptions must be met:

1. The material of the arch wire is linearly elastic.
2. After activating the closing loop, the material is still in the elastic range.
3. Displacement is small.
4. All arch wire forming the closing loop is in the same plane.
5. Distortion of the shape of the closing loop after activation is small.

It is obvious that either some or all of the assumptions 3 to 5 are violated in our application. Hence, we are not expecting good agreement with experimental results by employing Castigliano's theorem in loop analysis, as will be evident later. Nevertheless, trends indicating how to optimize the loop configuration are shown in the analytical solutions.

In general, there are three types of strain energy stored in the elastic body, namely, strain energy due to axial load, torsion, and bending. For the present types of closing loop applications, the torsional strain energy due to out-of-plane forces and strain energy due to axial loads are small as compared to its bending strain energy, hence the total strain energy can be approximately written as:

$$U = \frac{1}{2}\sum_i \int \frac{M_i^2 ds}{EI} \qquad (2)$$

where M_i is the bending moment of each basic element i of the loop, E, the Young's modulus of the arch wire material, I, the moment of inertia of cross-sectional area of the arch wire and ds, the differential length of the arch wire.

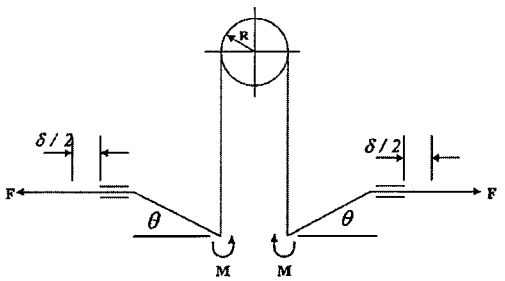

Fig. 1. Closing loop with gable bend angle activated by a force F

Consider the closing loop model as shown in Fig. 1 and from eqs. (1) and (2), the following relationships are obtained:

$$\delta = \frac{\partial U}{\partial F} = \frac{1}{2}\frac{\partial}{\partial F}\left[\sum_i \int \frac{M_i^2 ds}{EI}\right] \qquad (3)$$

$$\theta = \frac{\partial U}{\partial M} = \frac{1}{2}\frac{\partial}{\partial M}\left[\sum_i \int \frac{M_i^2 ds}{EI}\right] \qquad (4)$$

From eqs. (3) and (4), the expressions for the loop stiffness, $K = F/\delta$ and the moment-to-force ratio, M/F will be derived for each type of closing loop considered herein.

2.2 Vertical helical loop

For a vertical helical loop as shown in Fig. 2, the bending moment for each basic element of the loop is as follows:

$$M_1 = Fx - M \qquad 0 < x < H \qquad (5)$$

$$M_2 = F(H + R\sin\phi_1) - M \qquad 0 < \phi_1 < \pi \qquad (6)$$

$$M_3 = F(H - R\sin\phi_2) - M \qquad 0 < \phi_2 < \pi \qquad (7)$$

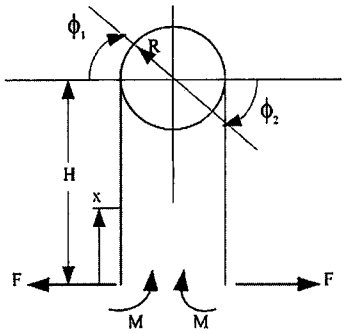

Fig. 2 Vertical helical loop

The strain energy for each element is:

$$U_1 = \frac{1}{2EI}\int_0^H (Fx - M)^2 dx \qquad (8)$$

$$U_2 = \frac{1}{2EI}\int_0^\pi [F(H + R\sin\phi_1) - M]^2 (Rd\phi_1) \qquad (9)$$

$$U_3 = \frac{1}{2EI}\int_0^\pi [F(H - R\sin\phi_2) - M]^2 (Rd\phi_2) \qquad (10)$$

Therefore the total strain energy of the vertical helical loop is:

$$U = 2U_1 + \left(\frac{N+1}{2}\right)U_2 + \left(\frac{N-1}{2}\right)U_3 \qquad (11)$$

where N is an odd number, the number of half-turns of the helices. For one helix N=3, with Castigliano's theorem according to eqs. (3) and (4), the following relationships are obtained:

$$\frac{M}{F} = \frac{H^2 + \pi NRH + 2R^2 + EI\theta/F}{2H + \pi NR} \qquad (12)$$

$$K = \frac{6EI}{4H^3 + 24HR^2 + 3\pi NR(2H^2 + R^2)} \qquad (13)$$

Eq. (13) coincides with that given by Haack [14] without the detail of derivation.

2.3 T-loop

For a T-loop as shown in Fig. 3, the bending moment for each basic element of the loop is as follows:

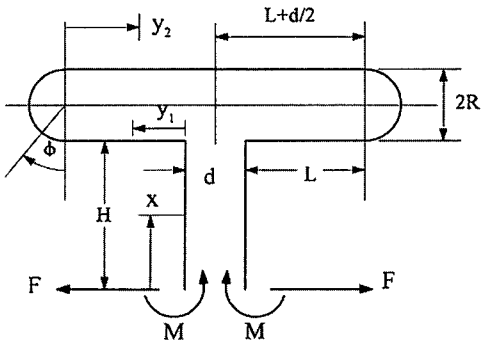

Fig. 3 T-loop

$$M_1 = Fx - M \qquad 0 < x < H \qquad (14)$$

$$M_2 = FH - M \qquad 0 < y_1 < L \qquad (15)$$

$$M_3 = F\left[H + R(1 - \cos\phi)\right] - M \qquad 0 < \phi < \pi \qquad (16)$$

$$M_4 = F(H + 2R) - M \qquad 0 < y_2 < (L + d/2) \qquad (17)$$

Therefore the total strain energy of the T-loop is:

$$EIU = \int_0^H (Fx - M)^2 dx + \int_0^L (FH - M)^2 dy_1 + \int_0^\pi [FH + FR(1 - \cos\phi) - M]^2 (Rd\phi) + \int_0^{L+d/2} [F(H + 2R) - M]^2 dy_2 \qquad (18)$$

Appling Castigliano's theorem according to eqs. (3) and (4), the following relationships are obtained:

$$\frac{M}{F} = [H^2 + 4L(H+R) + 2\pi R^2 + 2\pi RH + d(H+2R) + EI\theta/F]/[2H + 4L + 2\pi R + d] \quad (19)$$

$$K = 3EI/[2H^3 + 6H^2L + 6\pi RH^2 + 12\pi HR^2 + 9\pi R^3 + 3(2L+d)(H+2R)^2] \quad (20)$$

2.4 Opus90 loop

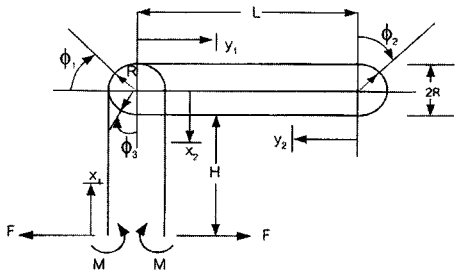

Fig. 4 Opus90 loop

Since the Opus90 loop is unsymmetrical, when it is centered within IBD (inter-bracket distance), the inherent moments anterior and posterior to both legs are not equal. For our purpose of deriving the formulae for loop optimization, we will assume that the Opus90 loop is located off-center such that the inherent moments at both legs are equal as shown in Fig. 4. The bending moment for each basic element of the loop is as follows:

$$M_1 = Fx_1 - M \qquad 0 < x_1 < H + R \quad (21)$$

$$M_2 = F[(H+R) + R\sin\phi_1] - M \qquad 0 < \phi_1 < \pi/2 \quad (22)$$

$$M_3 = F(H+2R) - M \qquad 0 < y_1 < L \quad (23)$$

$$M_4 = F[(H+2R) - R(1-\cos\phi_2)] - M \qquad 0 < \phi_2 < \pi \quad (24)$$

$$M_5 = FH - M \qquad 0 < y_2 < L \quad (25)$$

$$M_6 = F[H + R(1-\cos\phi_3)] - M \qquad 0 < \phi_3 < 3\pi/2 \quad (26)$$

$$M_7 = F[(H+R) - x_2] - M \qquad 0 < x_2 < H + R \quad (27)$$

Therefore the strain energy of the Opus90 loop is:

$$EIU = \frac{1}{2}\int_0^{H+R}(Fx_1 - M)^2 dx_1 + \frac{1}{2}\int_0^{\pi/2}[F(H+R+R\sin\phi_1) - M]^2 (Rd\phi_1) + \frac{1}{2}\int_0^{L}F[(H+2R) - M]^2 dy_1 + \frac{1}{2}\int_0^{\pi}[F\{(H+2R) - R(1-\cos\phi_2)\} - M]^2 (Rd\phi_2) + \frac{1}{2}\int_0^{L}(FH - M)^2 dy_2 + \frac{1}{2}\int_0^{3\pi/2}[F\{H + R(1-\cos\phi_3)\} - M]^2 (Rd\phi_3) + \int_0^{H+R}[F(H+R-x_2) - M]^2 dx_2 \quad (28)$$

Applying Castigliano's theorem to eq.(28) yields the following relationships:

$$\frac{M}{F} = [H^2(2+3\pi)RH + 3(1+\pi)R^2 + 2HL + 2RL + EI\theta/F]/[2(H+R) + 3\pi R + 2L] \quad (29)$$

$$K = 12EI/[8H^3 + 12(2+3\pi)H^2R + 72(1+\pi)HR^2 + (56+54\pi)R^3 + 24(2R^2L + 2RHL + H^2L)] \quad (30)$$

2.5 Helical T-loop

To obtain higher M/F ratio, in principle, we should locate the wire material as far from the base as possible. Hence, the authors are proposing a new configuration of loop, called a helical T-loop, as shown in Fig. 5. This configuration has been modified from the simple T-loop by adding helices at the upper wings. During derivation of the formulae any number of helices will be considered, but for practical purpose only one helix on each wing will be

analyzed later on. By increasing the length of the arch wire loop in this manner, it will result in greater flexibility, in other words, reduce the stiffness of the equivalent simple T-loop. This is a desirable loop property because the lower loop stiffness implies that the rate of force decays as the tooth moves to close the gap and will be slower. Hence, larger activation distance per patient visit can be achieved without causing severe stress and strain to the supporting structure of the tooth.

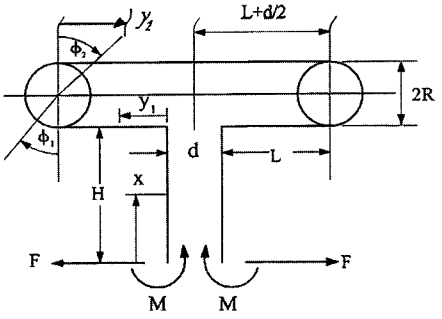

Fig. 5 Helical T-loop

The bending moment for each basic element of the helical T-loop is as follows:

$$M_1 = Fx - M \qquad 0 < x < H \qquad (31)$$

$$M_2 = FH - M \qquad 0 < y_1 < L \qquad (32)$$

$$M_3 = F\left[H + R\left(1 - \cos\phi_1\right)\right] - M \qquad 0 < \phi_1 < \pi \qquad (33)$$

$$M_4 = F\left[\left(H + 2R\right) - R\left(1 - \cos\phi_2\right)\right] - M \qquad 0 < \phi_2 < \pi \qquad (34)$$

$$M_5 = F\left(H + 2R\right) - M \qquad 0 < y_2 < L + d/2 \qquad (35)$$

The total strain energy of the helical T-loop is:

$$U = 2\left[U_1 + U_2 + \left(\frac{N+1}{2}\right)U_3 + \left(\frac{N-1}{2}\right)U_4 + U_5\right] \qquad (36)$$

where N is an odd number, the number of half-turns of the helices, and the strain energy for each basic element is as follows:

$$U_1 = \frac{1}{2EI}\int_0^H (Fx - M)^2\,dx \qquad (37)$$

$$U_2 = \frac{1}{2EI}\int_0^L (FH - M)^2\,dy_1 \qquad (38)$$

$$U_3 = \frac{1}{2EI}\int_0^\pi [F\left\{H + \mathrm{R}(1 - \cos\phi_1)\right\} - M]^2 (Rd\phi_1) \qquad (39)$$

$$U_4 = \frac{1}{2EI}\int_0^\pi [F\left\{(H + 2R) - \mathrm{R}(1 - \cos\phi_2)\right\} - M]^2 (Rd\phi_2) \qquad (40)$$

$$U_5 = \frac{1}{2EI}\int_0^{L+d/2} \left[F(H + 2R) - M\right]^2 dy_2 \qquad (41)$$

Observe from eq.(36) that for a simple T-loop N = 1, one helix N = 3, and two helices N = 5, applying Castigliano's theorem to eq. (36) and the following relationships are obtained:

$$\frac{M}{F} = [H^2 + 4L(H + R) + 2\pi NR^2 + 2\pi NRH + d(H + 2R) + EI\theta / F]/[2H + 4L + 2\pi NR + d] \qquad (42)$$

$$K = 3EI/[2H^3 + 6H^2L + 6\pi RH^2 + 12\pi HR^2 + 3(2L + d)(H + 2R)^2 + 9\pi NR^3] \qquad (43)$$

3. Results and discussion

3.1 Theoretical findings

The aim in investigating the theoretical results of each loop type is to find the optimum loop configuration to yield the highest ratio of M/F. The material of the arch wire is assumed to be stainless steel of cross-sectional area 0.016x0.022 inch (0.40x0.55 mm) whose Young's modulus is equal to 172,000 MPa. The size of any closing loop will be constrained by the anatomy of the oral cavity. For example, the total height of the loop is limited by the maximum height from the bracket on the tooth crown to the vestibule. Since it is known that the higher the loop, the higher the ratio of M/F will be achieved [4,15], therefore in the following investigation the total height and width (H_TxW) will be 10x10 mm for upper canine retraction.

The obtained optimum configuration will be used in experiments and analysis by FEM in part II of this paper.

3.2 Vertical helical loop

To find the optimum configuration, we assume that there is no gable bend angle θ in eq. (12) and consider only one helix in Fig. 2. The geometrical constraint equation is:

$$H+R = 10 \qquad (44)$$

The calculated results for each helix radius using eq. (12) yield the following:

R = 0.5 mm, H = 9.5 mm, M/F = 5.71 mm
R = 1.0 mm, H = 9.0 mm, M/F = 6.11 mm
R = 1.5 mm, H = 8.5 mm, M/F = 6.32 mm
R = 2.0 mm, H = 8.0 mm, M/F = 6.39 mm

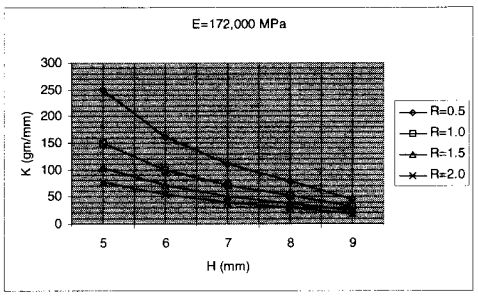

Fig. 6 Effect of helical radii on stiffness of vertical helical loop

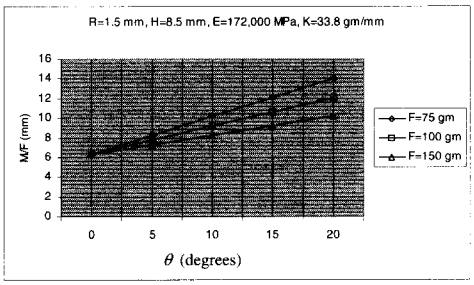

Fig. 7 M/F of vertical helical loop with gable bend

It is seen that the larger the helix radius , the higher ratio of M/F is obtained. But for a practical purpose, we choose to limit the maximum radius to R = 1.5 mm. The loop stiffness K can be calculated by using eq. (13) and the results are shown in Fig. 6. Notice that the larger the values of H or R, the lower the stiffness K will be. The optimum configuration is summarized as follows:

R = 1.5 mm, H = 8.5 mm, M/F = 6.32 mm, K = 33.8 gm/mm

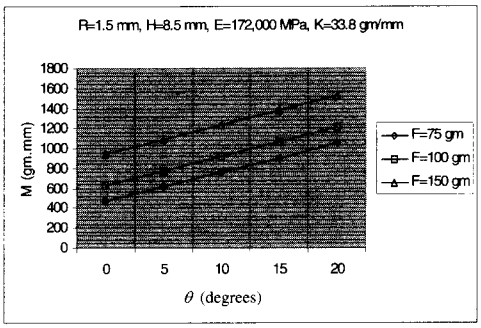

Fig. 8 Moments of vertical helical loop with gable bend

To see the effect of the gable bend angle, eq. (12) is used to construct Fig. 7 for various magnitudes of activating forces F and their corresponding moments M are shown in Fig. 8. In Part II, the more reliable FEM will be used to construct the same graph as Fig. 7 to demonstrate the right trend. This confirmation of the correct trend will be done for all four types of closing loop.

3.3 T-loop

To find the optimum configuration of the T-loop, we assume that there is no gable bend angle θ in eq. (19). The geometrical constraint equation according to Fig. 3 is:

$$H+2R = 10 \qquad (45)$$
$$2L+2R+d = 10 \qquad (46)$$

First we investigate the influence of d by arbitrarily fixing R = 1 mm. Then eqs. (45) and (46) become:

$$H = 8 \qquad (47)$$
$$2L+d = 8 \qquad (48)$$

Now the ratios of M/F are calculated by eq. (19) for d = 0, 1, and 2 mm to give:

d = 0 mm, H = 8, L = 4 mm, M/F = 6.91 mm
d = 1 mm, H = 8, L = 3.5 mm, M/F = 6.88 mm
d = 2 mm, H = 8, L = 3 mm, M/F = 6.85 mm

It is seen that d = 0 mm gives the highest value of M/F. However, observe that the influence of d on M/F is negligible. Also constructing a closing loop with d = 0 mm will facilitate the measurement of each activating of distance and the monitoring of the movement of the tooth. Now the constraint equations are reduced to:

$$H+2R = 10 \quad (49)$$
$$L+R = 5 \quad (50)$$

To search for optimum configuration from eqs. (49) and (50), we try R = 0.5, 1.0, and 1.5 mm and the following results are obtained:

R = 0.5 mm, H = 9 mm, L = 4.5 mm, M/F = 7.20 mm
R = 1.0 mm, H = 8 mm, L = 4.0 mm, M/F = 6.91 mm
R = 1.5 mm, H = 7 mm, L = 3.5 mm, M/F = 6.62 mm

From the above results, the smallest R yields the highest M/F. But for practical hand-bending of the closing loop, the smallest R is chosen to be 1.0 mm, hence the optimum configuration for T-loop is:

R = 1.0 mm, H = 8 mm, L = 4.0 mm, M/F = 6.91 mm, K = 23.8 gm/mm

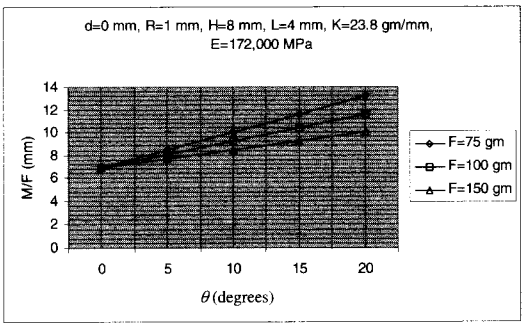

Fig. 9 M/F of T-loop with gable bend

To see the effect of the gable bend angle on M/F, eq. (19) is used to construct Fig. 9 for various magnitudes of activating forces F and their corresponding moments M are shown in Fig. 10. Since loop stiffness is also an important factor in determining the magnitude of activating distance per patient visit, the influences of the loop H and arch wire sizes on the loop stiffness are also shown in Fig. 11.

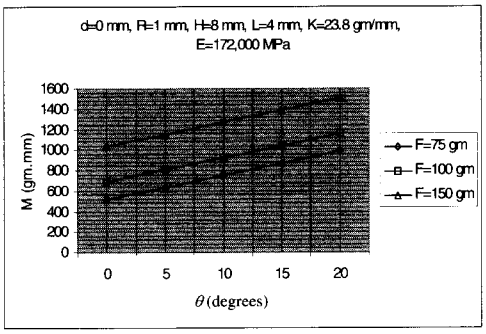

Fig. 10 Moments of T-loop with gable bend

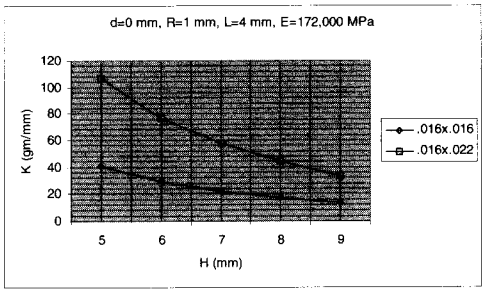

Fig. 11 Effect of arch wire size on stiffness of T-loop

3.4 Opus90 loop

For the Opus90 loop as shown in Fig. 4, the geometrical constraint equations are:

$$H+2R = 10 \quad (51)$$
$$L+2R = 10 \quad (52)$$

Following the similar procedure as the T-loop using eqs. (29) and (30), the optimum configuration is derived as follows:

R = 1.0 mm, H = 8 mm, L = 8 mm, M/F = 7.18 mm, K = 19.6 gm/mm

Here again the minimum radius R is limited to 1.0 mm for practical hand-bending of the loop. The effect of the gable bend angle on M/F for various magnitudes of activating forces F

and their corresponding moments are shown in Fig. 12 and 13. The influences of the loop height H and arch wire sizes on the loop stiffness are demonstrated in Fig. 14.

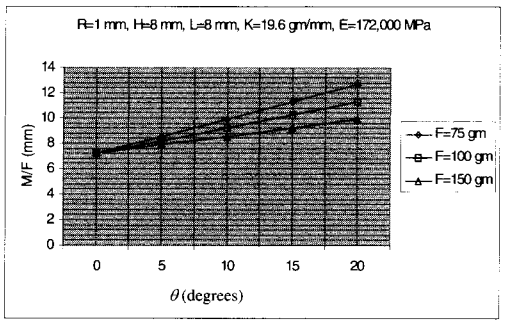

Fig. 12 M/F of Opus90 loop with gable bend

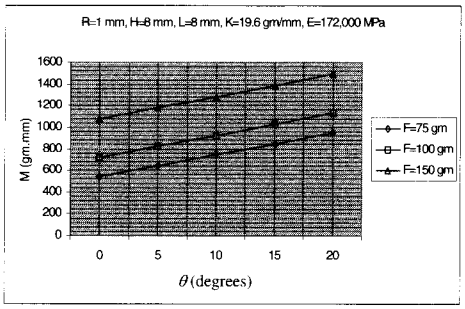

Fig. 13 Moments of Opus90 loop with gable bend

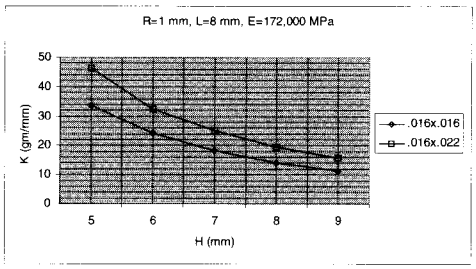

Fig. 14 Effect of arch wire sizes on stiffness of Opus90 loop

3.5 Helical T-loop

For the helical T-loop as shown in Fig. 5, the geometrical constraint equations are:

$$H+2R = 10 \quad (53)$$

$$2L+2R+d = 10 \quad (54)$$

Following a similar procedure as the T-loop using eqs. (42) and (43) for one helix, the optimum configuration is obtained as follows:

d = 0 mm, R = 1.0 mm, H = 8 mm, L = 4 mm, M/F = 7.43 mm, K = 23.5 gm/mm

The effect of the gable bend angle on M/F for various magnitudes of activating forces F and their corresponding moments are shown in Fig. 15 and 16. The influences of the loop height H and arch wire sizes on the loop stiffness are demonstrated in Fig. 17.

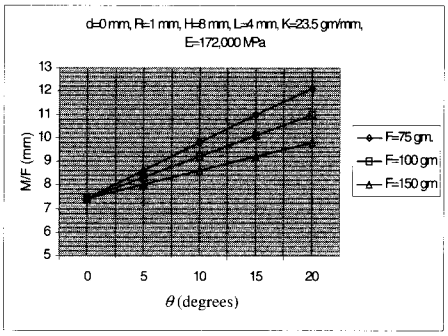

Fig. 15 M/F of helical T-loop with gable bend

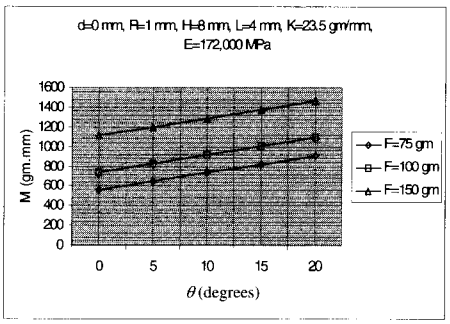

Fig. 16 Moments of helical T-loop with gable bend

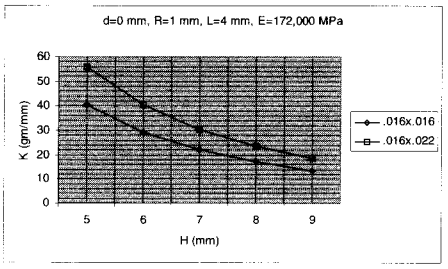

Fig. 17 Effect of arch wire sizes on stiffness of helical T-loop

4. Conclusion

In Part I of the paper, the theoretical derivations of the ratios of M/F and loop stiffness of four types of loop configurations have been shown in details. For maximum M/F, the results indicate that if one is required of to increase the loop height (H), the loop width (L), and use the smallest loop radius (R), except for the vertical helical loop, the largest loop radius is the best. This coincides with the observation of several researchers [1,4,6,15-19]. Experiments to compare the loop stiffness will be done in Part II. The results of the more reliable FEM will be presented for all optimum loop configurations obtained in Part I.

5. References

[1] Siatkowski, R. E. Continuous Arch wire Closing Loop Design, Optimization and Verification: Part I. Am J Orthod Dentofac Orthop, Vol.112, pp. 393-402 (October 1997).

[2] Burstone, C. J., Pryputniewicz, R. J., and Bowley, W. W. Holographic Measurement of Tooth Mobility in three Dimensions. J Periodontal Res, Vol. 13, pp.283-294, (July 1978).

[3] Pryputniewicz, R. J., and Burstone, C. J. The Effect of Time and Force Magnitude on Orthodontic Tooth Movement. J Dent Res, Vol. 58, pp. 1754-1764, (August 1979).

[4] Gjessing P. Biomechanical Design and Clinical Evaluation of a New Canine-Retraction Spring. Am J Orthod, Vol. 87, pp. 353-362, (May 1985).

[5] Burstone, C. J., and Goldberg, A. J. Beta Titanium: a New Orthodontic Alloy. Am J Orthod, Vol. 77, pp. 121-132, (February 1980).

[6] Hilgers, J. J., and Farzin-Nia, F. Adjuncts to Bioprogressive Therapy: the Asymmetrical "T" Arch wire. J Clin Orthod, Vol. 26, pp. 81-86, (February 1992).

[7] Siatkowski, R. E. Continuous arch wire Closing Loop Design, Optimization and Verification: Part II. Am J Orthod Dentofac Orthop, Vol. 112, pp. 487-495, (November 1997).

[8] Dermaut, L. R., Kleutghen, J. P. J., and De Clerck, H. J. J. Experimental Determination of the Center of Resistance of the Upper First Molar in a Macerated, dry Human Skull Submitted to Horizontal Headgear Traction. Am J Orthod, Vol. 90 pp. 29-36, (July 1986).

[9] Tanne, k., Sakuda, M., and Burstone, C. J. Three-dimension Finite Element Analysis for Stress in the Periodontal Tissue by Orthodontic Forces. Am J Orthod Dentofac Orthop, Vol. 92 pp. 499-505, (December 1987).

[10] Tanne, K., Koenig, H. A., and Burstone, C. J. Moment to Force Ratios and the Center of Rotation. Am J Orthod Dentofac Orthop, Vol. 94 pp. 426-431, (November 1988).

[11] Pedersen, E. H., Andersen, K. L., and Melsen, B. Tooth Displacement Analyzed on Human Autopsy Material by Means of a Strain Gauge Technique. Eur J Orthod, Vol. 13, pp. 65-74, (February 1991).

[12] Andersen, K. L., Pedersen, E. H., and Melsen, B. Material Parameters and Stress Profiles Within the Periodontal Ligament. Am J Orthod Dentofac Orthop, Vol. 99, pp. 427-440, (May 1991).

[13] Hibbeler, R. C. Mechanics of Materials. 4th ed. Upper Saddle River, NJ: Prentice Hall International, 2000.

[14] Haack, D. C. The Science of Mechanics and its Importance to Analysis and Research in the Field of Orthodontics. Am J Orthod, Vol. 49, pp. 330-344, (May 1963).

[15] Burstone, C. J., and Koenig, H. A. Optimizing Anterior and Canine Retraction. Am J Orthod, Vol. 70, pp. 1-19, (July 1976).

[16] Burstone, C. J., Steenbergen, E. V., Hanley, K. J. Modern Edgewise Mechanics and the Segmented Arch Technique. Glendora, CA: Ormco, 1995.

[17] Proffit, W. R., and Fields, H. W., Jr. Contemporary Orthodontics. St. Louis, MO: C. V. Mosby, 1993.

[18] Charles, C. R., and Jones, M. L. Canine Retraction with the Edgewise Appliance: Some Problems and Solutions. Br J Orthod, Vol. 9, pp. 194-202, (October 1982).

[19] Shaw, M. M., and Waters, N. E. The Characteristics of the Ricketts Maxillary Canine Retractor. Eur J Orthod, Vol. 14, pp. 37-46, (February 1992).